Chemical Science

ROYAL SOCIETY OF CHEMISTRY

EDGE ARTICLE

View Article Online
View Journal | View Issue

Check for updates

Cite this: *Chem. Sci.*, 2023, **14**, 1781

All publication charges for this article have been paid for by the Royal Society of Chemistry

Received 23rd October 2022
Accepted 17th January 2023

DOI: 10.1039/d2sc05857j

rsc.li/chemical-science

Open Access Article. Published on 19 January 2023. Downloaded on 12/28/2025 9:37:58 PM.
This article is licensed under a Creative Commons Attribution-NonCommercial 3.0 Unported Licence.

A nickel(II)-based one-dimensional organic–inorganic halide perovskite ferroelectric with the highest Curie temperature†

Hao-Fei Ni,‡[a] Lou-Kai Ye,‡[a] Peng-Cheng Zhuge,[a] Bo-Lan Hu,[a] Jia-Rui Lou,[a] Chang-Yuan Su,[b] Zhi-Xu Zhang,[b] Li-Yan Xie,*[a] Da-Wei Fu*[ab] and Yi Zhang*[ab]

Organic–inorganic halide perovskites (OIHPs) are very eye-catching due to their chemical tunability and rich physical properties such as ferroelectricity, magnetism, photovoltaic properties and photoluminescence. However, no nickel-based OIHP ferroelectrics have been reported so far. Here, we designed an ABX_3 OIHP ferroelectric (3-pyrrolinium)$NiCl_3$, where the 3-pyrrolinium cations are located on the voids surrounded by one-dimensional chains composed of $NiCl_6$-face-sharing octahedra *via* hydrogen bonding interactions. Such a unique structure enables the (3-pyrrolinium)$NiCl_3$ with a high spontaneous polarization (P_s) of 5.8 μC cm^{-2} and a high Curie temperature (T_c) of 428 K, realizing dramatic enhancement of 112 and 52 K compared to its isostructural (3-pyrrolinium)MCl_3 (M = Cd, Mn). To our knowledge, remarkably, (3-pyrrolinium)$NiCl_3$ should be the first case of nickel(II)-based OIHP ferroelectric to date, and its T_c of 428 K (35 K above that of $BaTiO_3$) is the highest among all reported one-dimensional OIHP ferroelectrics. This work offers a new structural building block for enriching the family of OIHP structures and will inspire the further exploration of new nickel(II)-based OIHP ferroelectrics.

Introduction

Organic–inorganic halide perovskites (OIHPs) have caught phenomenal research attention in recent years for their promising application potential in photovoltaics,[1] photoelectricity,[2,3] light emitting diodes,[4] ferroelectric memory,[5,6] and electron spin devices.[7,8] Among them, ferroelectrics feature switchable spontaneous polarization that acts as the essential core in nonvolatile memory, capacitors and sensors, *etc.*[9–14] OIHPs have occupied an important position in the ferroelectric field by taking advantage of their chemical tunability, light weight, mechanical flexibility and so on, compared with their inorganic counterparts. Structurally, OIHPs with the typical ABX_3-type (A = organic cation, B = metal cation, and X = halide anion) formula generally adopt two structural forms, either a three-dimensional BX_6-corner-sharing cubic structure or a one-dimensional BX_6-face-sharing hexagonal structure.[15–17] The A-site organic cations are embedded in the voids surrounded by the inorganic framework of BX_6 octahedra *via* weak interactions, endowing the OIHPs with great structural diversity and chemical variability.[18–23] Such unique structural characteristics open a rich platform for design synthesis and performance optimization of ferroelectric materials.[24–33] Nevertheless, hundreds of ABX_3-type OIHPs have been discovered, while only a few cases show ferroelectricity. Exploring reliable design concepts to assemble OIHP structures for developing high-performance ferroelectrics is an imminent ongoing challenge.

To be a ferroelectric, the crystal must have polar symmetry, whose polarization switching is inseparable from the reorientational arrangement of molecular dipoles in lattice. Accordingly, several design strategies involving chemical modifications on organic cations of OIHPs have been proposed to efficiently obtain molecular ferroelectrics.[34–36] For example, by modifying some structurally flexible building blocks, like spherical $[(CH_3)_4N]^+$, 1,4-diazabicyclo[2.2.2]octonium (Dabco) and quinuclidine, to be suitable A-site cations, a series of OIHP ferroelectrics have been designed with superior performance such as multiple polarization axes, large piezoelectric response and high Curie temperature (T_c).[37–45] Emphatically, a high T_c is essential for ferroelectric applications because it directly determines the working temperature range in many areas. Besides the organic cation itself, the weak interactions between organic and inorganic components in OIHPs cannot be ignored, which play an important role in crystallographic engineering to induce desired physical properties.[46–49] Previous studies have demonstrated the rational modifications on A-site organic cations to modulate weak interactions to realize the design and performance optimization of

[a]*Institute for Science and Applications of Molecular Ferroelectrics, Key Laboratory of the Ministry of Education for Advanced Catalysis Materials, Zhejiang Normal University, Jinhua, 321004, China. E-mail: liyanxie@zjnu.edu.cn; dawei@zjnu.edu.cn; yizhang1980@seu.edu*

[b]*Jiangsu Key Laboratory for Science and Applications of Molecular Ferroelectrics, Southeast University, Nanjing, 211189, China*

† Electronic supplementary information (ESI) available: Fig. S1–S7, Table S1–S4. CCDC 2214383 and 2214384. For ESI and crystallographic data in CIF or other electronic format see DOI: https://doi.org/10.1039/d2sc05857j

‡ These authors have contributed equally to this work.

© 2023 The Author(s). Published by the Royal Society of Chemistry

Open Access Article. Published on 19 January 2023. Downloaded on 12/28/2025 9:37:58 PM.
This article is licensed under a Creative Commons Attribution-NonCommercial 3.0 Unported Licence.

OIHP ferroelectrics such as (4,4-difluorohexahydroazepine)$_2$PbI$_4$,[37] and (ethylammonium)$_2$(EA)$_2$Pb$_3$Br$_{10}$.[50] In this stage, it has to be mentioned that, however, the BX_6 inorganic components in OIHPs are equally important while they are always easily overlooked under the halo of organic components. BX_6 octahedra in the reported ferroelectric OIHPs also have considerable diversity, with a variety of optional B-site metal ions such as Pb^{2+}, Mn^{2+}, Cd^{2+}, Cr^{2+}, Sn^{2+} and so on.[51–58] Notably, Xiong *et al.* reported a special nickel(II) nitrite-based organic–inorganic hybrid perovskite ferroelectric, [*N*-fluoromethyl tropine][Ni(NO$_2$)$_3$], designed by rational chemical modification and structural assembly.[59] Zhang *et al.* also reported several zero-dimensional packing phase transition materials with the Ni(NCS)$_6$ framework.[60] For nickel(II) halide crystals, a series of perovskite variants ABX_3 (B = Ni, A = Gu, FA, MA, X = Cl, Br; B = Mn, A = MA, X = Br) have been demonstrated to show optical properties and high electronic capacity ($CH_3NH_3NiCl_3$).[61,62] However, no nickel(II) halide-based OIHP ferroelectrics have been reported so far.

In the OIHP system, particularly, the 3-pyrrolinium cation has been shown to be a very promising candidate and an effective functional unit for building ferroelectrics, as reported in several previous studies such as (3-pyrrolinium)$CdBr_3$ and (3-pyrrolinium)MCl_3 (M = Cd, Mn).[29,55,56] On the other hand, compared to Mn(II) and Cd(II), the six-coordinated Ni(II) with a smaller radius can form a smaller nickel(II) halide octahedron with a reduced octahedron volume, which may compress the space for organic cation movements and reduce the distance of hydrogen bonding interactions, thereby resulting in high phase transition temperature. Accordingly, through an elaborate structural assembly, we here present a new nickel(II)-based OIHP ferroelectric, (3-pyrrolinium)$NiCl_3$, with a high T_c of 428 K, above that (about 393 K) of the inorganic perovskite ferroelectric $BaTiO_3$.[63] Systematic characterization reveals its remarkable ferroelectricity with a high saturated polarization (P_s) of 5.8 μC cm^{-2}, and the order–disorder transition of the 3-pyrrolinium cations which leads to a ferroelectric phase transition. Compared to its isostructural compounds previously reported, (3-pyrrolinium)MCl_3 (M = Cd, Mn) (Scheme 1),[55,56] the variation of the inorganic framework of BX_6 octahedra enables the T_c to get a significant increase of 112 and 52 K, due to the stronger hydrogen bonding interactions that act as a rope between the 3-pyrrolinium cations and $[NiCl_3]^-$ anionic chains. Moreover, to our knowledge, (3-pyrrolinium)$NiCl_3$ should be the first case of nickel(II)-based OIHP ferroelectric to date, which could provide a new structural paradigm for one-dimensional ABX_3 OIHP ferroelectrics. More importantly, its T_c of 428 K is the highest among all reported one-dimensional OIHP ferroelectrics, making it competitive for ferroelectric-related devices with a wide operating temperature range.

Results and discussion

(3-Pyrrolinium)$NiCl_3$ was prepared by the reaction of 3-pyrrolinium chloride and nickel chloride in dilute hydrochloric acid solution, and its prism-like colorless crystals were easily obtained by a slow solution evaporating method. The preliminary differential scanning calorimetry (DSC) traces show a pair of endothermic/exothermic peaks in the heating/cooling runs (Fig. 1), indicating a reversible phase transition at about 428 K (Curie temperature, T_c), higher than those of the analogous (3-pyrrolinium)$CdCl_3$ (T_c = 316 K) and (3-pyrrolinium)$MnCl_3$ (T_c = 376 K).

To understand the phase transition mechanism and ferroelectric origin of (3-pyrrolinium)$NiCl_3$, we determined its crystal structures and the resulting crystal data at various temperatures are summarized in Table S1.† (3-Pyrrolinium)$NiCl_3$ adopts a one-dimensional hexagonal ABX_3-type perovskite structure, where the infinite linear chains of the face-sharing $NiCl_6$ octahedron along the [0 0 1] direction are separated by the A-site 3-pyrrolinium cations (Fig. 2). The anion chains and organic cations are loosely connected by N–H···Cl hydrogen bonding interactions. At room temperature in the phase below T_c (marked as LTP), the (3-pyrrolinium)$NiCl_3$ crystallized in an orthorhombic space group $Cmc2_1$ (polar point group *mm*2) with the well-ordered 3-pyrrolinium cations and distorted $NiCl_6$ octahedra. From the packing view of the crystal structure, all of the 3-pyrrolinium cations are aligned along the *c*-axis, which could result in a spontaneous polarization. On the basis of the point charge model for (3-pyrrolinium)$NiCl_3$ in LTP (Fig. S1†), the estimated spontaneous polarization along the [0 0 1] direction is about 6.08 μC cm^{-2}. In the phase above T_c (marked as HTP), the crystal symmetry of (3-pyrrolinium)$NiCl_3$ transforms into the centrosymmetric space group *Cmcm*, which belongs to the point group *mmm*. Such crystallographic symmetry of *mmm* cancels out the molecular dipoles in each direction, leading to zero macroscopic polarization. In the HTP, the 3-pyrrolinium cations are located on the special symmetry site of 2*mm* in the lattice, and

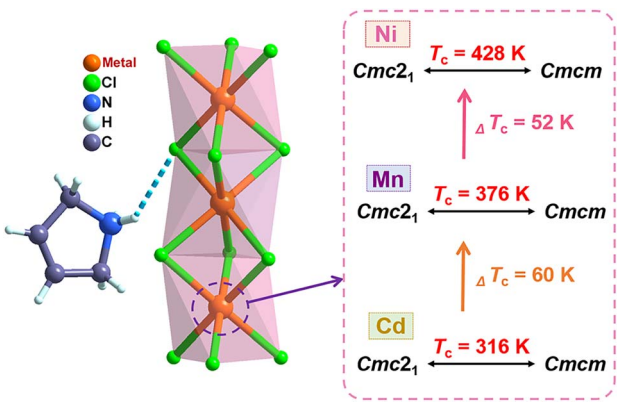

Scheme 1 The design concept of ferroelectric (3-pyrrolinium)$NiCl_3$ with the one-dimensional ABX_3 OIHP structure.

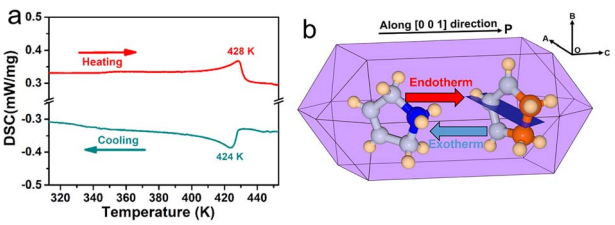

Fig. 1 (a) DSC curves of (3-pyrrolinium)$NiCl_3$ in heating/cooling runs. (b) Simulative single crystal shape of (3-pyrrolinium)$NiCl_3$.

© 2023 The Author(s). Published by the Royal Society of Chemistry

Open Access Article. Published on 19 January 2023. Downloaded on 12/28/2025 9:37:58 PM.
This article is licensed under a Creative Commons Attribution-NonCommercial 3.0 Unported Licence.

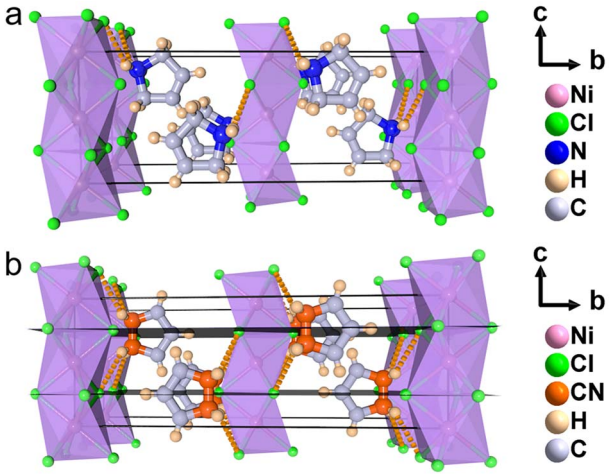

Fig. 2 Packing view of crystal structures of (3-pyrrolinium)$NiCl_3$ in (a) LTP and (b) HTP. The orange dotted lines represent N–H···Cl hydrogen bonding, and the black plane represents mirror symmetry elements.

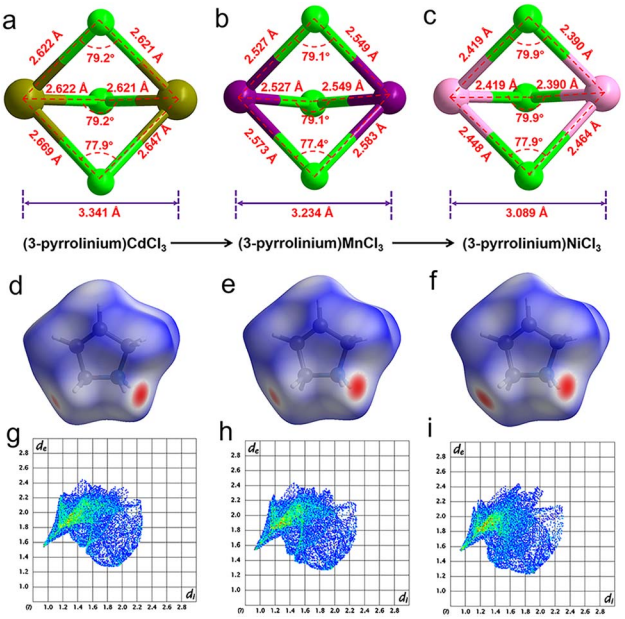

Fig. 3 Comparison of anionic chains of (a) (3-pyrrolinium)$CdCl_3$, (b) (3-pyrrolinium)$MnCl_3$ and (c) (3-pyrrolinium)$NiCl_3$. The Hirshfeld d_{norm} surfaces (d–f) and two-dimensional (2D) fingerprint plots (g–i) for the 3-pyrrolinium cations in (3-pyrrolinium)MCl_3 (M = Cd, Mn, Ni). The d_i of the x-axis coordinate and the d_e of the y-axis represent the distance (\) from the atoms inside the cation to the Hirshfeld surface and the external atoms to the Hirshfeld surface respectively.

consequently the cations are required to show 2-fold orientational disorder, where the C and N atoms distribute equally in two positions by the mirror plane symmetry perpendicular to the *c*-axis. The anion chains of the $NiCl_6$ octahedron experience little change except the octahedron become more regular. Therefore, the phase transition mechanism can be mainly attributed to the order–disorder transition of 3-pyrrolinium cations. From HTP to LTP, the symmetric elements are halved from eight (E, i, C_2, $2C_2'$, σ_h, $2\sigma_v$) in HTP to four (E, C_2, $2\sigma_v$) in LTP (Fig. S2†). The symmetry breaking occurs with the disappearance of the mirror element, leading to the orientational ordering of cations to generate spontaneous polarization, which means that the (3-pyrrolinium)$NiCl_3$ is an *mmmFmm*2-type ferroelectric with two equivalent polarization directions.

The stacking structure and phase transition mechanism of (3-pyrrolinium)$NiCl_3$ are similar to those of (3-pyrrolinium)MCl_3 (M = Cd, Mn), while the T_c has been greatly improved to up to 428 K. This would be closely associated with the changes of hydrogen-bonding interactions by different inorganic anion chains, and then affect the energy barrier of cationic orientational motions. As shown in Fig. 3a–c, for (3-pyrrolinium)MCl_3 (M = Cd, Mn, Ni), the M–Cl bond distances undergo a decrease in sequence from Cd, Mn to Ni, with the range changes from 2.621–2.669 \ to 2.527–2.583 \ to 2.390–2.464 \. Obviously, the MCl_6 (M = Cd, Mn, Ni) octahedra gradually become smaller with the variable M–M distances in anion chains from 3.341 \ to 3.234 \ to 3.089 \. The M–M distances between adjacent anion chains also experienced a gradual decrease with the changes of MCl_6 octahedra from Cd, Mn to Ni (Fig. S3†). These changes make the void smaller, resulting in a confinement effect to increase the energy for cation rotation (Table S2†). Based on the Density Functional Theory (DFT) calculations, the energy barrier for the rotation of 3-pyrrolinium cations in (3-pyrrolinium)MCl_3 (M = Cd, Mn, Ni) are 4.27, 4.51, and 4.97 eV respectively (Fig. S4–S7 and Table S3†), which indicates that (3-pyrrolinium)$NiCl_3$ has a higher T_c, consistent with the results for structural analysis. In the OIHP system, besides the anionic component, hydrogen bonding interactions also have to be considered, which have been utilized as an indispensable tool in crystal engineering to design desired physical properties. The N–H···Cl hydrogen-bonding in (3-pyrrolinium)$NiCl_3$ is stronger than the other two compounds, which can be clearly seen from the shortest distance between the donor (N) and acceptor (Cl) in (3-pyrrolinium)MCl_3 (M = Cd, Mn, Ni) with 3.335, 3.306 and 3.302 \ respectively (Fig. S3†). The Hirshfeld d_{norm} surfaces and related 2D fingerprint plots of 3-pyrrolinium cations in (3-pyrrolinium)MCl_3 (M = Cd, Mn, Ni) were further calculated to get the information about the environment of cations and intermolecular contacts (Fig. 3d–i).

From the Hirshfeld d_{norm} surfaces, the short contacts (represented by the deep red circular depressions on the surfaces) between the cation and its surroundings for (3-pyrrolinium)$NiCl_3$ are closer than those for (3-pyrrolinium)MCl_3 (M = Cd, Mn), which are reflected in 2D fingerprints by quantifying the mean d_{norm} value for (3-pyrrolinium)$NiCl_3$ (0.384), (3-pyrrolinium)$MnCl_3$ (0.422) and (3-pyrrolinium)$MnCl_3$ (0.424). The calculated results show that the total interactions in (3-pyrrolinium)$NiCl_3$ are stronger than those in (3-pyrrolinium)MCl_3 (M = Cd, Mn), which like a strong rope pull the cations, leading to a larger energy barrier required for the structural phase transition of (3-pyrrolinium)$NiCl_3$.

Ferroelectric phase transitions are generally accompanied by significant anomalies of dielectric permittivity at around T_c. For (3-pyrrolinium)$NiCl_3$, the real part ε' of the complex dielectric constant exhibits a sharp λ-shaped peak-like response at about T_c = 428 K in each frequency (Fig. 4a). The peak values are several

Open Access Article. Published on 19 January 2023. Downloaded on 12/28/2025 9:37:58 PM. This article is licensed under a Creative Commons Attribution-NonCommercial 3.0 Unported Licence.

hundred to one thousand times larger than those in the stable state. We also carried out the second harmonic generation (SHG) measurements to study the symmetry changes of (3-pyrrolinium)$NiCl_3$ during ferroelectric phase transition, by taking advantage of the high sensitivity of the SHG response to the breaking of the space-inversion symmetry. The SHG signal shows non-zero intensity in LTP (ferroelectric phase), consistent with the polar space group $Cmc2_1$, and experiences a change with temperature increasing until T_c (Fig. 4b). Above T_c, the SHG signal becomes inactive and maintains the zero intensity in HTP (paraelectric phase), corresponding to the centrosymmetric space group *Cmcm*.

The ferroelectricity with polarization reversal of (3-pyrrolinium)$NiCl_3$ was directly verified by measuring polarization–electric field (*P*–*E*) hysteresis loops (Fig. 5). A linear *P*–*E* curve was obtained at 443 K above its T_c, indicating that it is currently in the paraelectric phase. On cooling to 428 K at about T_c, the result begins to show a compressed S-shaped curve. And then, the *P*–*E* curve opens to form a typical loop at 423 K below T_c, entering the ferroelectric phase. Upon further cooling, the ferroelectric loops expand and the P_r (remnant polarization) value increases gradually to reach about 5.8 μC cm^{-2} at 303 K, in accordance with the estimated value of 6.08 μC cm^{-2} from the crystal structure. The measured saturated polarization (P_s) and remnant polarization (P_r) values are close to each other. The polarization value of 5.8 μC cm^{-2} is higher than those of the ABX_3-type OIHP ferroelectrics reported thus far (Table S4†), and larger than that of the reported nickel(II) nitrite-based hybrid perovskite ferroelectric [*N*-fluoromethyl tropine][$Ni(NO_2)_3$] (3.0 μC cm^{-2}). Moreover, its T_c of 428 K should be the highest among all reported one-dimensional OIHP ferroelectrics (Table S4†), which combined with the small coercive field E_c in the range of 2.6–4.8 kV cm^{-1}, makes (3-pyrrolinium)$NiCl_3$ more competitive for relatively high-temperature, low operation voltage, low-power information storage devices.

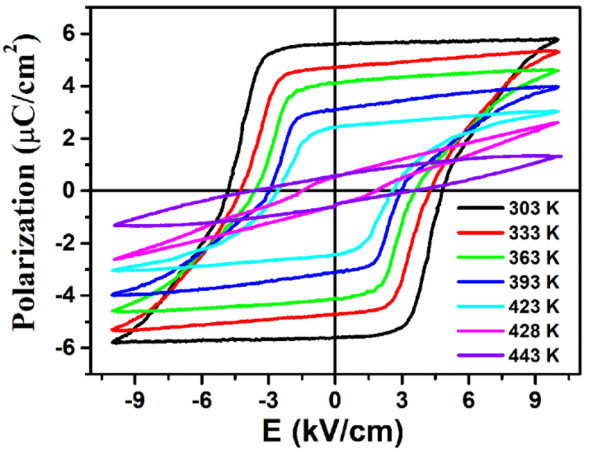

Fig. 5 Ferroelectric hysteresis loops of (3-pyrrolinium)$NiCl_3$ measured at different temperatures in the LTP.

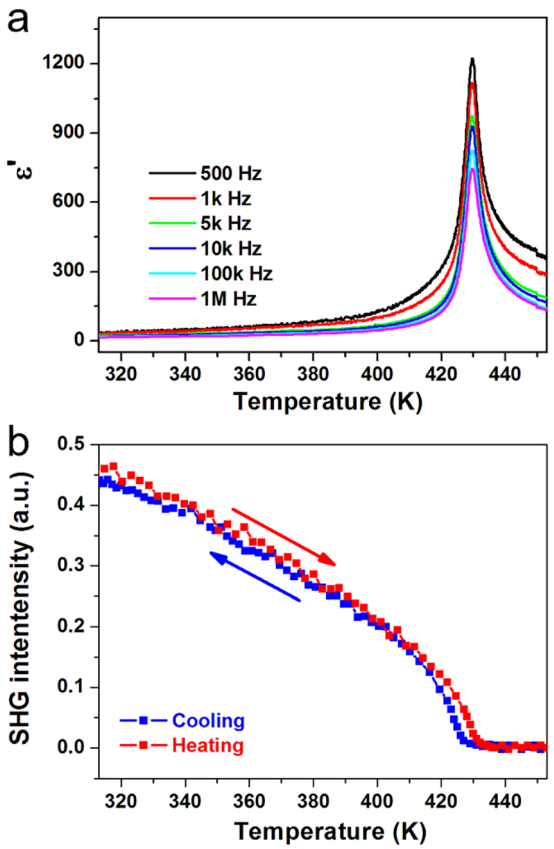

Fig. 4 Temperature-dependent (a) real part of the complex dielectric constant and (b) SHG intensity of (3-pyrrolinium)$NiCl_3$.

Conclusions

In summary, we successfully designed a new nickel(II)-based OIHP ferroelectric, (3-pyrrolinium)$NiCl_3$, through an elaborate structural assembly of 3-pyrrolinium organic cations and one-dimensional $[NiCl_3]_n^-$ chains of $NiCl_6$-face-sharing octahedra. It undergoes an *mmmFmm*2-type ferroelectric phase transition at 428 K, induced by the thermally driven transition of 3-pyrrolinium cations. The confined environment of 3-pyrrolinium cations caused by anion chains and relatively strong hydrogen bonding interactions give rise to a high energy barrier for phase transition, inducing ferroelectricity up to a high Curie temperature of 428 K. To our knowledge, such a T_c of 428 K should be the highest among all reported one-dimensional OIHP ferroelectrics, offering a wide operating temperature range for ferroelectric-related devices. More strikingly, (3-pyrrolinium)$NiCl_3$ is the first nickel(II)-based OIHP ferroelectric, enriching the hybrid perovskite ferroelectric families. Considering the structural diversity and chemical tunability of OIHPs, one can expect more such nickel(II)-based OIHPs to be discovered with excellent ferroelectricity.

Author contributions

H.-F. N. conceived the experiments and wrote the paper. L.-K. Y., P.-C. Z. G., B.-L. H. and J.-R. L. performed the experiments. C.-Y. S. and Z.-X. Z. assisted in the auxiliary analysis of data. L.-Y. X., D.-W. F. and Y. Z. guided and supervised this work.

© 2023 The Author(s). Published by the Royal Society of Chemistry

Open Access Article. Published on 19 January 2023. Downloaded on 12/28/2025 9:37:58 PM. This article is licensed under a Creative Commons Attribution-NonCommercial 3.0 Unported Licence.

Conflicts of interest

The authors declare no conflict of interest.

Acknowledgements

This work was financially supported by the National Natural Science Foundation of China (grant 21991141) and Zhejiang Normal University. The authors acknowledge the financial support from the Open Research Fund of the Key Laboratory of the Ministry of Education for Advanced Catalysis Materials and Zhejiang Key Laboratory.

Notes and references

1 A. K. Jena, A. Kulkarni and T. Miyasaka, *Chem. Rev.*, 2019, **119**, 3036–3103.
2 H. Wang and D. H. Kim, *Chem. Soc. Rev.*, 2017, **46**, 5204–5236.
3 Y. Zhao, C. Li and L. Shen, *InfoMat*, 2019, **1**, 164–182.
4 L. N. Quan, B. P. Rand, R. H. Friend, S. G. Mhaisalkar, T.-W. Lee and E. H. Sargent, *Chem. Rev.*, 2019, **119**, 7444–7477.
5 W.-J. Xu, S. Kopyl, A. Kholkin and J. Rocha, *Coord. Chem. Rev.*, 2019, **387**, 398–414.
6 H.-Y. Zhang, X.-J. Song, X.-G. Chen, Z.-X. Zhang, Y.-M. You, Y.-Y. Tang and R.-G. Xiong, *J. Am. Chem. Soc.*, 2020, **142**, 4925–4931.
7 B. Huang, J.-Y. Zhang, R.-K. Huang, M.-K. Chen, W. Xue, W.-X. Zhang, M.-H. Zeng and X.-M. Chen, *Chem. Sci.*, 2018, **9**, 7413–7418.
8 K. Liao, X. Hu, Y. Cheng, Z. Yu, Y. Xue, Y. Chen and Q. Gong, *Adv. Opt. Mater.*, 2019, **7**, 1900350.
9 X.-G. Chen, X.-J. Song, Z.-X. Zhang, P.-F. Li, J.-Z. Ge, Y.-Y. Tang, J.-X. Gao, W.-Y. Zhang, D.-W. Fu, Y.-M. You and R.-G. Xiong, *J. Am. Chem. Soc.*, 2020, **142**, 1077–1082.
10 X. Li, F. Wu, Y. Yao, W. Wu, C. Ji, L. Li, Z. Sun, J. Luo and X. Liu, *J. Am. Chem. Soc.*, 2022, **144**, 14031–14036.
11 W.-Q. Liao, D. Zhao, Y.-Y. Tang, Y. Zhang, P.-F. Li, P.-P. Shi, X.-G. Chen, Y.-M. You and R.-G. Xiong, *Science*, 2019, **363**, 1206–1210.
12 M. E. Lines and A. M. Glass, *Principles and applications of ferroelectrics and related materials*, Oxford University Press, 2001.
13 L. P. Miao, N. Ding, N. Wang, C. Shi, H. Y. Ye, L. Li, Y. F. Yao, S. Dong and Y. Zhang, *Nat. Mater.*, 2022, **21**, 1158–1164.
14 J. F. Scott, *Science*, 2007, **315**, 954–959.
15 T. Chen, Y. Zhou, Z. Sun, S. Zhang, S. Zhao, Y. Tang, C. Ji and J. Luo, *Inorg. Chem.*, 2015, **54**, 7136–7138.
16 A. Kojima, K. Teshima, Y. Shirai and T. Miyasaka, *J. Am. Chem. Soc.*, 2009, **131**, 6050–6051.
17 K. Liu, Y. Jiang, Y. Jiang, Y. Guo, Y. Liu and E. Nakamura, *J. Am. Chem. Soc.*, 2019, **141**, 1406–1414.
18 P.-Z. Huang, H.-F. Ni, C.-Y. Su, M.-M. Lun, H.-F. Lu, D.-W. Fu and Q. Guo, *CCS Chem.*, 2022, 1–10.
19 Q. Jia, T. Shao, L. Tong, C. Su, D. Fu and H. Lu, *Chin. Chem. Lett.*, 2022, DOI: **10.1016/j.cclet.2022.05.053**.
20 W. Li, Z. Wang, F. Deschler, S. Gao, R. H. Friend and A. K. Cheetham, *Nat. Rev. Mater.*, 2017, **2**, 16099.
21 W.-Q. Liao, Y.-Y. Tang, P.-F. Li, Y.-M. You and R.-G. Xiong, *J. Am. Chem. Soc.*, 2018, **140**, 3975–3980.
22 B. Saparov and D. B. Mitzi, *Chem. Rev.*, 2016, **116**, 4558–4596.
23 C.-Y. Su, Y. Yao, Z. Zhang, Y. Wang, M. Chen, P.-Z. Huang, Y. Zhang, W. Qiao and D.-W. Fu, *Chem. Sci.*, 2022, **13**, 4794–4800.
24 Y. Ai, X.-G. Chen, P.-P. Shi, Y.-Y. Tang, P.-F. Li, W.-Q. Liao and R.-G. Xiong, *J. Am. Chem. Soc.*, 2019, **141**, 4474–4479.
25 H. L. B. Boström, M. S. Senn and A. L. Goodwin, *Nat. Commun.*, 2018, **9**, 2380.
26 K. Gesi, *J. Phys. Soc. Jpn.*, 1990, **59**, 432–434.
27 Y. Hu, K. Parida, H. Zhang, X. Wang, Y. Li, X. Zhou, S. A. Morris, W. H. Liew, H. Wang, T. Li, F. Jiang, M. Yang, M. Alexe, Z. Du, C. L. Gan, K. Yao, B. Xu, P. S. Lee and H. J. Fan, *Nat. Commun.*, 2022, **13**, 5607.
28 Y. Hu, L. You, B. Xu, T. Li, S. A. Morris, Y. Li, Y. Zhang, X. Wang, P. S. Lee, H. J. Fan and J. Wang, *Nat. Mater.*, 2021, **20**, 612–617.
29 P.-F. Li, W.-Q. Liao, Y.-Y. Tang, H.-Y. Ye, Y. Zhang and R.-G. Xiong, *J. Am. Chem. Soc.*, 2017, **139**, 8752–8757.
30 M.-M. Lun, T. Zhang, C.-Y. Su, J. Li, Z.-X. Zhang, D.-W. Fu and H.-F. Lu, *Mater. Chem. Front.*, 2022, **6**, 1929–1937.
31 X. J. Song, T. Zhang, Z. X. Gu, Z. X. Zhang, D. W. Fu, X. G. Chen, H. Y. Zhang and R. G. Xiong, *J. Am. Chem. Soc.*, 2021, **143**, 5091–5098.
32 H. Wei, Y. Yang, S. Chen and H. J. Xiang, *Nat. Commun.*, 2021, **12**, 637.
33 Y. Zhang, H.-Y. Ye, W. Zhang and R.-G. Xiong, *Inorg. Chem. Front.*, 2014, **1**, 118–123.
34 H.-Y. Zhang, Y.-Y. Tang, P.-P. Shi and R.-G. Xiong, *Acc. Chem. Res.*, 2019, **52**, 1928–1938.
35 T. Zhang, K. Xu, J. Li, L. He, D.-W. Fu, Q. Ye and R.-G. Xiong, *Natl. Sci. Rev.*, 2022, DOI: **10.1093/nsr/nwac240**.
36 Z.-X. Zhang, H.-Y. Zhang, W. Zhang, X.-G. Chen, H. Wang and R.-G. Xiong, *J. Am. Chem. Soc.*, 2020, **142**, 17787–17794.
37 X.-G. Chen, X.-J. Song, Z.-X. Zhang, H.-Y. Zhang, Q. Pan, J. Yao, Y.-M. You and R.-G. Xiong, *J. Am. Chem. Soc.*, 2020, **142**, 10212–10218.
38 D. W. Fu, J. X. Gao, W. H. He, X. Q. Huang, Y. H. Liu and Y. Ai, *Angew. Chem., Int. Ed.*, 2020, **59**, 17477–17481.
39 J.-X. Gao, W.-Y. Zhang, Z.-G. Wu, Y.-X. Zheng and D.-W. Fu, *J. Am. Chem. Soc.*, 2020, **142**, 4756–4761.
40 W.-Q. Liao, Y.-Y. Tang, P.-F. Li, Y.-M. You and R.-G. Xiong, *J. Am. Chem. Soc.*, 2017, **139**, 18071–18077.
41 Y.-Y. Tang, Y. Xie, Y.-L. Zeng, J.-C. Liu, W.-H. He, X.-Q. Huang and R.-G. Xiong, *Adv. Mater.*, 2020, **32**, 2003530.
42 C.-F. Wang, H. Li, M.-G. Li, Y. Cui, X. Son, Q.-W. Wang, J.-Y. Jiang, M.-M. Hua, Q. Xu, K. Zhao, H.-Y. Ye and Y. Zhang, *Adv. Funct. Mater.*, 2021, **31**, 2009457.
43 Y.-M. You, W.-Q. Liao, D. Zhao, H.-Y. Ye, Y. Zhang, Q. Zhou, X. Niu, J. Wang, P.-F. Li, D.-W. Fu, Z. Wang, S. Gao, K. Yang, J.-M. Liu, J. Li, Y. Yan and R.-G. Xiong, *Science*, 2017, **357**, 306–309.
44 J. Ma, Q. Xu, L. Ye, Q. Wang, Z. Gong, C. Shi, H. Ye and Y. Zhang, *J. Rare Earths*, 2022, **40**, 937–941.

© 2023 The Author(s). Published by the Royal Society of Chemistry

Open Access Article. Published on 19 January 2023. Downloaded on 12/28/2025 9:37:58 PM.
This article is licensed under a Creative Commons Attribution-NonCommercial 3.0 Unported Licence.

45 C. F. Wang, C. Shi, A. Zheng, Y. Wu, L. Ye, N. Wang, H. Y. Ye, M. G. Ju, P. Duan, J. Wang and Y. Zhang, *Mater. Horiz.*, 2022, **9**, 2450–2459.
46 F. F. Awwadi, R. D. Willett, K. A. Peterson and B. Twamley, *Chem.–Eur. J.*, 2006, **12**, 8952–8960.
47 L. Zhang, X. Liu, J. Li and S. McKechnie, *Sol. Energy Mater. Sol. Cells*, 2018, **175**, 1–19.
48 T. Zhang, K. Ding, J. Y. Li, G. W. Du, L. L. Chu, Y. Zhang and D. W. Fu, *Chin. J. Chem.*, 2022, **40**, 1559–1565.
49 Y. Zhao, P. Zhu, S. Huang, S. Tan, M. Wang, R. Wang, J. Xue, T.-H. Han, S.-J. Lee, A. Zhang, T. Huang, P. Cheng, D. Meng, J.-W. Lee, J. Marian, J. Zhu and Y. Yang, *J. Am. Chem. Soc.*, 2020, **142**, 20071–20079.
50 Y. Liu, S. Han, J. Wang, Y. Ma, W. Guo, X.-Y. Huang, J.-H. Luo, M. Hong and Z. Sun, *J. Am. Chem. Soc.*, 2021, **143**, 2130–2137.
51 Y. Ai, R. Sun, Y.-L. Zeng, J.-C. Liu, Y.-Y. Tang, B.-W. Wang, Z.-M. Wang, S. Gao and R.-G. Xiong, *Chem. Sci.*, 2021, **12**, 9742–9747.
52 Q. Pan, Z.-B. Liu, Y.-Y. Tang, P.-F. Li, R.-W. Ma, R.-Y. Wei, Y. Zhang, Y.-M. You, H.-Y. Ye and R.-G. Xiong, *J. Am. Chem. Soc.*, 2017, **139**, 3954–3957.
53 C.-F. Wang, H. Li, Q. Ji, C. Ma, L. Liu, H.-Y. Ye, B. Cao, G. Yuan, H.-F. Lu, D.-W. Fu, M.-G. Ju, J. Wang, K. Zhao and Y. Zhang, *Adv. Funct. Mater.*, 2022, **32**, 2205918.
54 W.-J. Xu, C.-T. He, C.-M. Ji, S.-L. Chen, R.-K. Huang, R.-B. Lin, W. Xue, J.-H. Luo, W.-X. Zhang and X.-M. Chen, *Adv. Mater.*, 2016, **28**, 5886–5890.
55 H.-Y. Ye, Y. Zhang, D.-W. Fu and R.-G. Xiong, *Angew. Chem., Int. Ed.*, 2014, **53**, 11242–11247.
56 H.-Y. Ye, Q. Zhou, X. Niu, W.-Q. Liao, D.-W. Fu, Y. Zhang, Y.-M. You, J. Wang, Z.-N. Chen and R.-G. Xiong, *J. Am. Chem. Soc.*, 2015, **137**, 13148–13154.
57 H.-Y. Zhang, X.-G. Chen, Z.-X. Zhang, X.-J. Song, T. Zhang, Q. Pan, Y. Zhang and R.-G. Xiong, *Adv. Mater.*, 2020, **32**, 2005213.
58 Y. Zhang, W.-Q. Liao, D.-W. Fu, H.-Y. Ye, C.-M. Liu, Z.-N. Chen and R.-G. Xiong, *Adv. Mater.*, 2015, **27**, 3942–3946.
59 Y.-A. Xiong, T.-T. Sha, Q. Pan, X.-J. Song, S.-R. Miao, Z.-Y. Jing, Z.-J. Feng, Y.-M. You and R.-G. Xiong, *Angew. Chem., Int. Ed.*, 2019, **58**, 8857–8861.
60 Z.-H. Jia, J.-Y. Liu, D.-X. Liu, S.-Y. Zhang, Z.-Y. Du, C.-T. He, W.-X. Zhang and X.-M. Chen, *J. Mater. Chem. C*, 2021, **9**, 8076–8082.
61 M. Daub, I. Ketterer and H. Hillebrecht, *Z. Anorg. Allg. Chem.*, 2018, **644**, 280–287.
62 L. T. Lopez, D. Ramirez, F. Jaramillo and J. A. Calderon, *Electrochim. Acta*, 2020, **357**, 136882.
63 G. H. Haertling, *J. Am. Chem. Soc.*, 1999, **82**, 797–818.

© 2023 The Author(s). Published by the Royal Society of Chemistry